Astronomy & Astrophysics manuscript no. biosig
October 23, 2020

Coexistence of CH_4, CO_2 and H_2O in exoplanet atmospheres

P. Woitke[1,2], O. Herbort[1,2,3], Ch. Helling[1,2,4], E. Stüeken[1,3], M. Dominik[1,2], P. Barth[1,2,3], and D. Samra[1,2]

[1] Centre for Exoplanet Science, University of St Andrews, St Andrews, UK
[2] SUPA, School of Physics & Astronomy, University of St Andrews, St Andrews, KY16 9SS, UK
[3] School of Earth & Environmental Studies, University of St Andrews, St Andrews, KY16 9AL, UK
[4] SRON Netherlands Institute for Space Research, Sorbonnelaan 2, 3584 CA Utrecht, NL

Received 08/07/2020; accepted 17/10/2020

ABSTRACT

We propose a classification of exoplanet atmospheres based on their H, C, O, N element abundances below about 600 K. Chemical equilibrium models were run for all combinations of H, C, N, O abundances, and three types of solutions were found, which are robust against variations of temperature, pressure and nitrogen abundance. Type A atmospheres contain H_2O, CH_4, NH_3 and either H_2 or N_2, but only traces of CO_2 and O_2. Type B atmospheres contain O_2, H_2O, CO_2 and N_2, but only traces of CH_4, NH_3 and H_2. Type C atmospheres contain H_2O, CO_2, CH_4 and N_2, but only traces of NH_3, H_2 and O_2. Other molecules are only present in ppb or ppm concentrations in chemical equilibrium, depending on temperature. Type C atmospheres are not found in the solar system, where atmospheres are generally cold enough for water to condense, but exoplanets may well host such atmospheres. Our models show that graphite (soot) clouds can occur in type C atmospheres in addition to water clouds, which can occur in all types of atmospheres. Full equilibrium condensation models show that the outgassing from warm rock can naturally provide type C atmospheres. We conclude that type C atmospheres, if they exist, would lead to false positive detections of biosignatures in exoplanets when considering the coexistence of CH_4 and CO_2, and suggest other, more robust non-equilibrium markers.

Key words. planets and satellites: atmospheres – planets and satellites: composition – astrochemistry

1. Introduction

The detection of exoplanets that exhibit spectral signatures of biological activity (biosignatures) is one of the most urgent goals of modern astronomy. Because of observational limitations, such biosignatures are currently based on certain combinations of abundant molecules that exhibit detectable spectroscopic signatures at medium spectral resolution in the infrared, such as H_2O, CO_2, CH_4 and CO. Other potentially abundant molecules like H_2, O_2 and N_2 have no permanent dipole moment and are more difficult to detect. Molecules generally need to have a minimum concentration of about 10^{-4} (100 ppm) to be detectable with the James Webb Space Telescope (JWST) (Krissansen-Totton et al. 2019; Sousa-Silva et al. 2020), and here a number of candidates have been discussed recently. For example, O_3 as an indicator for the presence of O_2 (Gaudi et al. 2018), SO_2-derived sulphate aerosols as an indicator for volcanic activity (Misra et al. 2015), or PH_3 as biosignature (Sousa-Silva et al. 2020).

Searching for suitable combinations of detectable molecules that suggest biological activity, Krissansen-Totton et al. (2019) have recently proposed to consider the coexistence of CO_2 and CH_4 (without CO) in planetary atmospheres, as is true for Earth (Meadows et al. 2018). In fact, CO_2 and CH_4 represent the two endpoints of the redox-spectrum of carbon, and it is hence not obvious why both molecules should be present simultaneously. Krissansen-Totton et al. (2018) argued that a disequilibrium between CH_4 and CO_2, accompanied by N_2 and liquid H_2O, was present during the Archean on Earth. Sandora & Silk (2020) review the evolutionary processes involving CH_4 in the Earth atmosphere. Once the specific geological processes cease that used to cause that disequilibrium, it seems unlikely that non-biological processes could maintain such an atmosphere on habitable exoplanets. However, Krissansen-Totton et al. did not explore in how far CO_2 and CH_4 can simply coexist in chemical equilibrium.

Previous chemical models in astronomy have mainly focused on H-rich atmospheres. For example, Moses et al. (2013) and Hu & Seager (2014) have presented sparse grids of chemical models varying the H abundance, metallicity and C/O-ratio to study the atmospheric composition of mini Neptune and super Earths, including kinetical quenching, photodissociation and vertical mixing. These papers show that carbon can mostly form CO_2 at low H abundances, rather than CO and CH_4 as used from the H_2-dominated atmospheres. Heng & Tsai (2016) have considered an analytic nine-molecule model in chemical equilibrium to discuss the effects of varying C/O and N/O ratios on H_2-dominated hot exoplanet atmospheres, aiming at a fast tool to retrieve the atmospheric composition from exoplanet observations. Morley et al. (2017) have considered chemical equilibrium models for the atmospheres of Earth-sized exoplanets including those of the TRAPPIST-1 system, based on element abundances taken from Venus, Earth and Titan, to discuss their observability with JWST.

Simulating the chemical evolution of the Earth atmosphere, (Zerkle et al. 2012) have identified the photo-dissociation of CH_4 as important non-equilibrium physical process in the upper atmosphere. The low dissociation energy of CH_4 (~4.3 eV) implies that this molecule can be dissociated quite easily compared to CO_2. Therefore, UV irradiation is thought to significantly change the atmospheric CH_4/CO_2 ratio over time (Zerkle et al. 2012), and if the hydrogen atoms (or H_2 molecules) can escape, which are produced by this reaction, the photo-dissociation of CH_4 is able to remove hydrogen from exoplanet atmospheres, creating more oxidising conditions. Arney et al. (2016) proposed that during the Archean, Earth was likely covered in photochem-

ical haze triggered by this process. Another large uncertainty here is the Earth's history of surface pressure and atmospheric N_2 abundance, which was possibly affected by the evolution of life as well (Stüeken et al. 2016).

The aim of this paper is to present an exhaustive study of the composition of exoplanet atmospheres considering all possible combinations of H, C, N and O abundances assuming chemical equilibrium. Substantial deviations from chemical equilibrium can be caused by biological activity, but other physical and geological processes may explain these disequilibria, too, for example UV and cosmic ray irradiation. But, in any case, potential biosignatures should not be based on combinations of molecules which are already expected in chemical equilibrium (Seager et al. 2013).

2. Simplified chemical equilibrium

All known atmospheres of solar system bodies are mainly composed of hydrogen (H), oxygen (O), carbon (C) and nitrogen (N), so we will focus on the H – C – N – O system in this paper, which is the most pressing system for the observational characterisation of exoplanets and the identification of possible biosignatures.

At low temperatures, $T \lesssim 600\,\mathrm{K}$, the Gibbs free energies $\Delta G_f = \Delta H_f - T\Delta S$ are dominated by the enthalpy of formation ΔH_f, which means that in chemical equilibrium, the molecular concentrations will essentially minimise ΔH_f. In Table 1 we list a few atomisation energies, i.e. the energies required to convert molecules into neutral atoms, for example $E_a(H_2O) = 2\Delta H_f(H) + \Delta H_f(O) - \Delta H_f(H_2O)$. The data have been extracted from the NIST-Janaf tables (Chase et al. 1982; Chase 1986).

Simple combinatorics shows that CH_4, CO_2, H_2O and N_2 are the thermodynamically most favourable molecules to minimise ΔH_f. For example, all of the following reactions are exothermic

$$\begin{aligned}
H_2 + \tfrac{1}{4}\,CO_2 &\longrightarrow \tfrac{1}{2}\,H_2O + \tfrac{1}{4}\,CH_4 && : -0.39\,\mathrm{eV}\\
CO + \tfrac{1}{2}\,H_2O &\longrightarrow \tfrac{3}{4}\,CO_2 + \tfrac{1}{4}\,CH_4 && : -0.81\,\mathrm{eV}\\
HCN + \tfrac{3}{4}\,H_2O &\longrightarrow \tfrac{3}{8}\,CO_2 + \tfrac{5}{8}\,CH_4 + \tfrac{1}{2}\,N_2 && : -1.51\,\mathrm{eV}\\
C_2H_2 + \tfrac{3}{2}\,H_2O &\longrightarrow \tfrac{3}{4}\,CO_2 + \tfrac{5}{4}\,CH_4 && : -2.56\,\mathrm{eV}\\
NH_3 + \tfrac{3}{8}\,CO_2 &\longrightarrow \tfrac{3}{4}\,H_2O + \tfrac{3}{8}\,CH_4 + \tfrac{1}{2}\,N_2 && : -2.83\,\mathrm{eV}\\
O_2 + \tfrac{1}{2}\,CH_4 &\longrightarrow H_2O + \tfrac{1}{2}\,CO_2 && : -4.17\,\mathrm{eV}
\end{aligned}$$

which means that all other molecules can react exothermally to eventually form a mixture of only CH_4, CO_2, H_2O and N_2 to minimise the Gibbs free energy at low temperatures. The first reaction requires to break a C-O bond, likely biologically mediated, and has been named "methanogenesis" by Woese & Fox (1977) and Waite et al. (2017). With increasing temperature, entropy becomes more relevant, and H_2 is the first among the trace molecules to reach significant concentrations, followed by CO.

Therefore, we first consider a planetary atmosphere in which the most abundant molecules are H_2O, CH_4, CO_2 and N_2 (henceforth called type C atmospheres), such that the total gas pressure is approximately given by

$$p_\mathrm{gas} \approx p_\mathrm{H2O} + p_\mathrm{CH4} + p_\mathrm{CO2} + p_\mathrm{N2}\,. \tag{1}$$

Table 1. Atomisation energies E_a of selected molecules

molecule	E_a at $T = 0\,K$	molecule	E_a at $T = 0\,K$
CH_4	17.02 eV	CO	11.11 eV
C_2H_2	16.86 eV	N_2	9.76 eV
CO_2	16.56 eV	H_2O	9.51 eV
HCN	13.09 eV	O_2	5.12 eV
NH_3	12.00 eV	H_2	4.48 eV

The element conservation equations can be expressed in terms of a fictitious total pressure after complete atomisation, p_atom, here $p_\mathrm{atom} = 3\,p_\mathrm{H2O} + 5\,p_\mathrm{CH4} + 3\,p_\mathrm{CO2} + 2\,p_\mathrm{N2}$,

$$H \cdot p_\mathrm{atom} = 2\,p_\mathrm{H2O} + 4\,p_\mathrm{CH4}\,, \quad C \cdot p_\mathrm{atom} = p_\mathrm{CO2} + p_\mathrm{CH4}\,, \tag{2}$$
$$O \cdot p_\mathrm{atom} = p_\mathrm{H2O} + 2\,p_\mathrm{CO2}\,, \quad N \cdot p_\mathrm{atom} = 2\,p_\mathrm{N2}\,, \tag{3}$$

where H, C, O and N are the given element abundances normalised by the condition $H + C + O + N = 1$. The usual element abundances in astronomy are defined with respect to hydrogen, for example $\epsilon_C = C/H$ and $\epsilon_O = O/H$, but here we wish to also consider hydrogen-poor atmospheres with $H \to 0$.

This system of linear equations, Eqs. (1) to (3), can be readily solved for the molecular partial pressures

$$\begin{aligned}
\frac{p_\mathrm{H2O}}{p_\mathrm{gas}} &= \frac{H + 2O - 4C}{H + 2O + 2N}\,, & \frac{p_\mathrm{CO2}}{p_\mathrm{gas}} &= \frac{2O + 4C - H}{2H + 4O + 4N}\,,\\
\frac{p_\mathrm{CH4}}{p_\mathrm{gas}} &= \frac{H - 2O + 4C}{2H + 4O + 4N}\,, & \frac{p_\mathrm{N2}}{p_\mathrm{gas}} &= \frac{2N}{H + 2O + 2N}\,.
\end{aligned} \tag{4}$$

If any of the partial pressures according to Eq. (4) is negative, we have obviously left the region of applicability of our assumptions. These side conditions are

$$O > 0.5\,H + 2\,C \quad \Rightarrow \quad O_2\text{-rich atmosphere, no } CH_4 \tag{5}$$
$$H > 2\,O + 4\,C \quad \Rightarrow \quad H_2\text{-rich atmosphere, no } CO_2 \tag{6}$$
$$C > 0.25\,H + 0.5\,O \quad \Rightarrow \quad \text{graphite condensation, no } H_2O\,. \tag{7}$$

We can furthermore use Eqs. (4) to determine where two of the molecular partial pressures are equal

$$H = 2\,O \quad \Longleftrightarrow \quad p_\mathrm{CO2} = p_\mathrm{CH4} \tag{8}$$
$$12\,C = 2\,O + 3\,H \quad \Longleftrightarrow \quad p_\mathrm{CO2} = p_\mathrm{H2O} \tag{9}$$
$$12\,C = 6\,O + H \quad \Longleftrightarrow \quad p_\mathrm{H2O} = p_\mathrm{CH4}\,. \tag{10}$$

The partial pressure of N_2 is always positive according to Eq. (4), providing no additional constraints. Hence, nitrogen does not interfere with the H – C – O system, unless there is a surplus of H according to Eq. (6), in which case NH_3 becomes an abundant molecule, see Sect. A.1.

3. Full chemical equilibrium models

To confirm the simplified analysis presented in Sect. 2, we ran full gas-phase chemical equilibrium models with GGchem (Woitke et al. 2018) for the elements H, C, N, and O. GGchem finds 52 molecular species in its database for this element mixture: H_2, C_2, N_2, O_2, CH, NH, OH, CN, CO, NO, HCN, CHNO, HCO, CH_2, H_2CO, CH_3, CH_4, CNO, CNN, NCN, CO_2, C_2H, C_2H_2, C_2H_4, C_2H_4O, C_2N, C_2N_2, C_2O, C_3, C_3O_2, C_4, C_4N_2, C_5, HNO, HONO, HNO_2, HNO_3, HO_2, NH_2, N_2H_2, H_2O, NH_3, N_2H_4, NO_2, NO_3, N_2O, N_2O_3, N_2O_4, N_2O_5, N_3, O_3 and C_3H. The results for $T = 400\,\mathrm{K}$ and $p = 1\,\mathrm{bar}$ are shown in Fig. 1. The region of coexistence of H_2O, CO_2 and CH_4 is indicated by a grey triangle corresponding to Eqs. (5) to (7), and the dashed lines of equal concentration correspond to Eqs. (8) to (10). The models have been computed with a small nitrogen abundance $N = 10^{-3}$, but the results are independent of N when plotted as function of $C/(H + O + C)$ and $(O - H)/(O + H)$, since nitrogen does not interfere significantly with the H – C – O system. See Appendix A for a discussion in how far our results depend on temperature, pressure, and nitrogen abundance.

These results show that, indeed, none of the other molecules are relevant to this problem. N_2, H_2O, CO_2 and CH_4 are the only

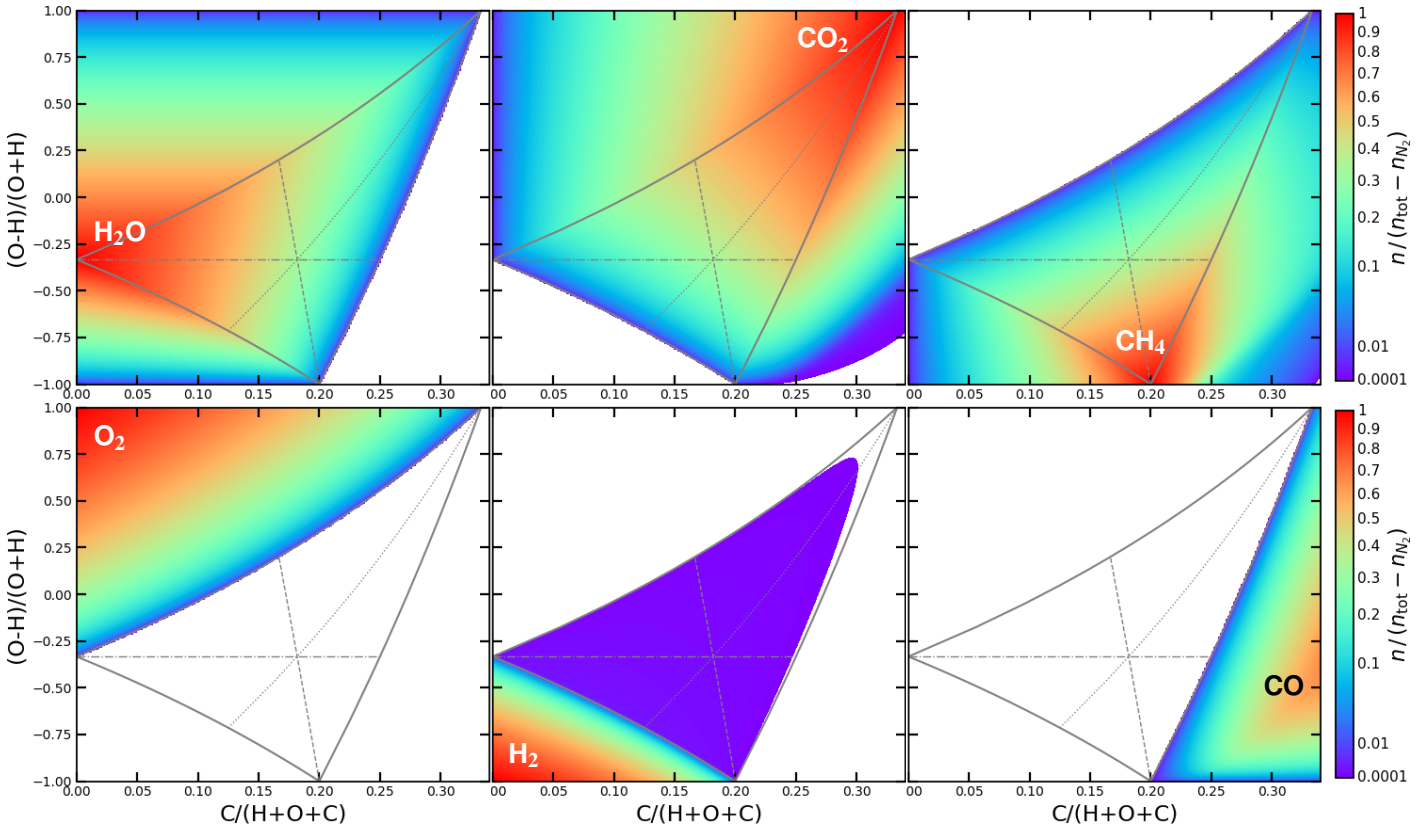

Fig. 1. Molecular concentrations in chemical equilibrium as function of H, C and O element abundances, calculated for $T = 400$ K and $p = 1$ bar. The central grey triangle marks the region within which H_2O, CH_4 and CO_2 coexist in chemical equilibrium. The thin grey lines indicate where two concentrations are equal: $n_{H_2O} = n_{CO_2}$ (dashed), $n_{CO_2} = n_{CH_4}$ (dash-dotted), and $n_{CH_4} = n_{H_2O}$ (dotted). n means particle densities. Blank regions have concentrations $< 10^{-4}$. In order to enhance the colour contrasts, a colour-map was chosen that is linear in $(n/(n_{tot} - n_{N_2}))^{1/2}$ from 0.01 to 1.

Table 2. Trace gas concentrations in chemical equilibrium with element abundances $N = 2/13$, $H = 6/13$, $O = 3/13$ and $C = 2/13$, where main constituents are 25% N_2, 25% H_2O, 25% CO_2 and 25% CH_4.

	200 K	300 K	400 K	500 K	600 K	700 K
H_2	2 ppb	5.8 ppm	390 ppm	0.52%	2.9%	9.5%
CO	< 1 ppb	< 1 ppb	260 ppb	39 ppm	0.11%	1.2%
NH_3	205 ppb	4.7 ppm	23 ppm	58 ppm	101 ppm	130 ppm

molecules that must be considered within the grey triangle to solve the element conservation equations, at least approximately, and therefore the argumentation presented in Sect. 2 holds.

The patterns shown in Fig. 1 are robust against changes of pressure, temperature, and nitrogen abundance, see Appendix A for details. This is the true strength of this diagram. All results can be approximately inferred just from the identification and stoichiometry of the four most stable molecules, making these results suitable for a classification of exoplanet atmospheres. The central triangle shows trace concentrations of H_2 on a level of a few 10^{-4} at 400 K, otherwise the gas composition is very pure in chemical equilibrium, with only three abundant molecules at any point besides N_2. With increasing temperature, the H_2 trace concentration increases, followed by the occurrence of CO in trace concentrations, see Table 2. Molecules not listed in Table 2 have even lower abundances. We conclude that the simplified analysis of the coexistence of H_2O, CO_2 and CH_4 as presented in Sect. 2 is valid to about 600 K.

The results of Moses et al. (2013) and Hu & Seager (2014, see their Figs. 4-6) show similar patterns, but their sparse grid of models and usage of H-abundance and C/O ratio make it difficult to compare their results with ours in detail.

4. Water and graphite condensation

GGchem also computes the supersaturation ratios of graphite C[s], liquid water H_2O[l], solid water H_2O[s], and the ices of ammonia NH_3[s], methane CH_4[s], CO[s] and CO_2[s]. While the ices only deposit at $T \lesssim 200$ K at 1 bar, the effect of carbon and water condensation is significant, see Fig. 2. Shaded areas in this diagram indicate that at least one condensed species is supersaturated ($S > 1$). Such gases are expected to form clouds, and the precipitation of cloud particles would remove the respective elements from the gas phase. Exoplanet atmospheres can hence not reside within the shaded areas, but are expected to move toward the edges of the blank regions in Fig. 2, where they come to rest.

However, the extent of the supersaturated areas depends on temperature, pressure and nitrogen abundance, and hence on atmospheric height, which complicates the analysis. Earth, for example, is not a point in Fig. 2, but a line, because the water content in the gas phase increases with temperature, guided by the condition $S(H_2O, T) \approx 1$.

Fig. 2 shows that at 350 K, 1 bar and small nitrogen abundance, the triangle in which H_2O, CO_2 and CH_4 coexist, is mostly covered by the supersaturated areas, either graphite or water or both. At 400 K, however, water cannot condense anywhere in the left diagram, and then the grey triangle of coexistence is only partly inhibited by graphite condensation. The grey triangle is less affected by supersaturation for lower pressures or increased nitrogen abundances. The occurrence of graphite clouds in exoplanet atmospheres was discussed, for example, by Moses et al. (2013, see their Fig. 7).

Figure 3 shows the results of some full equilibrium condensation models for 18 elements from Herbort et al. (2020). In these models, the total (= condensed + gas phase) element

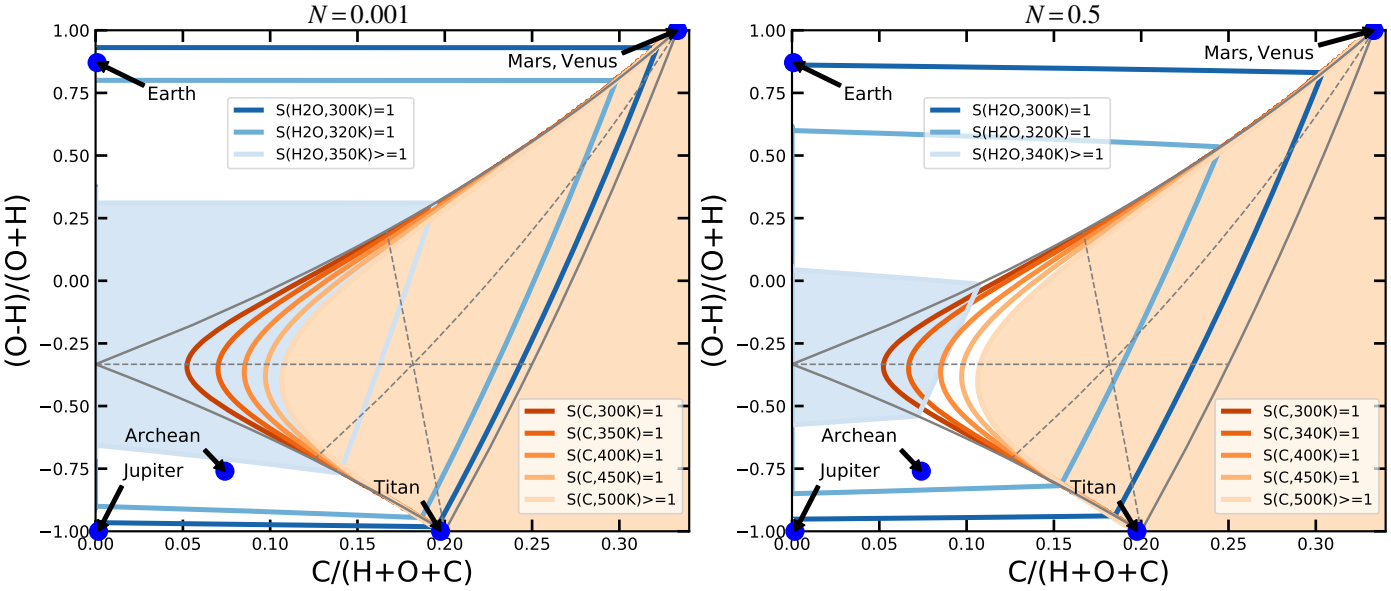

Fig. 2. Impact of liquid water (H_2O) and graphite (C) condensation at constant pressure of 1 bar. The blue and orange contour lines mark where the supersaturation ratio S equals one for water and graphite, respectively, at selected temperatures. Inside of the light blue and light orange shaded regions, the gas is supersaturated with respect to water at 350 K and graphite at 500 K, respectively. For higher temperatures, lower pressures or higher N abundances, the shaded areas shrink and eventually vanish. The left diagram is calculated for a small nitrogen abundance $N = 0.001$, whereas $N = 0.5$ is assumed in the right diagram. The atmospheric compositions of Earth, Mars, Venus, Jupiter, Titan and the Archean Earth (taken from Miller 1953) are marked. Earth (assuming 1.5% water content) sits right on top of the $S(H_2O, 300\,K, N = 0.5) = 1$ line.

abundances are taken from different materials found in the Earth crust, meteorites and polluted white dwarfs, see explanation of abbreviations in the figure caption. The model determines which liquid and solid materials are present at each temperature and subtracts the respective condensed element fractions, until $S \leq 1$ is achieved for all condensates. The remaining gas phase element abundances are plotted in Fig. 3 with lines, where we start at 600 K (circle) and follow the results down to 200 K. The changes of the H, O and C abundances along these tracks are caused by the effects of progressive condensation in these models, in particular phyllosilicates, carbonates, graphite and water. The CC model is very dry and eventually creates an almost pure N_2 atmosphere with some CO_2 at low temperatures. All other models eventually form a mixture of N_2 and CH_4, similar to Titan's atmosphere. In the MORB and BSE models, graphite condenses below 550 K and 600 K, respectively, but there is no liquid water. The PWD model shows neither graphite nor water condensation, but the CI and the water-enriched BSE models show liquid water at 369 K and 373 K, respectively, below which the models follow tracks, due to the removal of H_2O and C, along the borderline between type A and C, where the CO_2-concentration is low but still notable, for example the CI model at 350 K has 10% N_2, 48% CH_4, 42% H_2O and 0.35% CO_2.

In Fig. 3, we have additionally overplotted some simple equilibrium condensation models for the four element H, C, N, O only, where the initial element abundances are arbitrarily set as listed in Table 3. These models show the principle behaviour of type A, B and C atmospheres when only affected by water and graphite condensation. At ~ 350 K and 1 bar, the three type C models show similar abundances of CO_2 and CH_4, both with concentrations of a few percent, besides the major molecules N_2 and H_2O, next to liquid water.

5. Conclusions

A mixture of H_2O, CO_2, CH_4 and N_2 has been found to be the most favourable combination of molecules to minimise the Gibbs free energy at low temperatures $T \lesssim 600$ K. If all available elements can be converted into these molecules, the gas will only contain these species, whereas all other molecules only have trace concentrations in chemical equilibrium. However, if this is not possible, due to stoichiometric constraints, additional types of atmospheres occur:

A) Type A atmospheres are *H*-rich and mostly contain CH_4, H_2O and NH_3, but CO_2 and O_2 are lacking. In Appendix A.1 we show that the forth abundant molecule is either H_2 (type A1) or N_2 (type A2). The atmospheres of Jupiter, Titan and Archean Earth belong to type A. Titan's cold atmosphere is almost water-free because of condensation, but does have some H_2 (about 0.15%, Niemann et al. 2005).

B) Type B atmospheres are *O*-rich and mostly contain O_2, N_2, CO_2 and H_2O, but CH_4, NH_3 and H_2 are lacking. Earth belongs to this type. The Martian atmosphere is a members of type B, too, because it contains some O_2 (about 0.1%[1]), Venus is too hot for our classification, but its atmosphere is also mostly made of CO_2 and N_2, with traces of H_2O, but no CH_4 and no NH_3[1].

C) Type C atmospheres mostly contain H_2O, CO_2, CH_4 and N_2, but NH_3, H_2 and O_2 are lacking. This type of atmospheres was discussed in Sect. 2.

The molecule CO is not abundant in any type of atmosphere at low temperatures in chemical equilibrium.

Type C exoplanet atmospheres are not found in the solar system, possibly because the low temperatures of the objects favour water condensation, which reduces the hydrogen and oxygen abundances, however, slightly warmer exoplanets may well host such atmospheres. Type C atmospheres are featured by the coexistence of CH_4 and CO_2, both with percent-concentrations, which is possible in equilibrium only in type C atmospheres. Our models furthermore suggest that only in type C atmospheres, carbon can directly condense to form graphite (soot) clouds.

[1] See fact-sheets at https://nssdc.gsfc.nasa.gov/planetary.

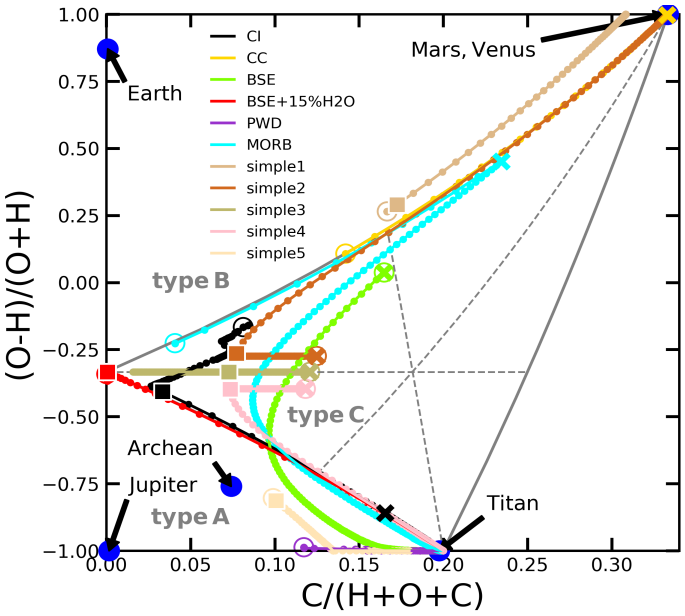

Fig. 3. Results from six full equilibrium condensation models for 18 elements from Herbort et al. (2020), re-computed for $p = 1$ bar, and five simple models for just 4 elements, see Table 3. Each model starts at $T = 600$ K (marked by circles) and then we follow that model with a line down to 200 K with 200 log-equidistant points. Abbreviations are carbonaceous chondrites (CI), Mid Oceanic Ridge Basalt (MORB), Continental Crust (CC), Bulk Silicate Earth (BSE), and abundances deduced from Polluted White Dwarf observations (PWD). The points where the trajectories start to have graphite are marked by crosses, and the points where liquid water starts to occur are marked by squares.

Table 3. Setup of simple equilibrium condensation models for four elements. T_C and T_{H2O} are the temperatures below which graphite and liquid water condense at 1 bar. The constant graphite condensation temperature of 600 K is because this is where we start our models.

	H	O	C	N	type	T_C [K]	T_{H2O} [K]
simple 1	0.28	0.48	0.15	0.09	B	–	348
simple 2	0.45	0.25	0.15	0.15	C	600	358
simple 3	0.47	0.23	0.15	0.15	C	600	358
simple 4	0.47	0.21	0.16	0.16	C	600	358
simple 5	0.64	0.07	0.08	0.21	A	–	337

The full equilibrium condensation models show that type C atmospheres can naturally be created by the outgassing from common rock materials such as carbonaceous chondrites (CI) or Mid Oceanic Ridge Basalt (MORB) at temperatures > 400 K. The two inner rocky planets of the Trappist-1 planet system, with estimated surface temperatures of about 370 K and 320 K, respectively (Morley et al. 2017), might host such atmospheres, and will be observed with the James Webb Space Telescope, see details in Turbet et al. (2020).

Biosignatures: The identification of spectral signatures of biological activity needs to proceed via two steps. First, identify combinations of molecules which cannot co-exist in chemical equilibrium ("non-equilibrium markers"). Second, find biological processes that cause such dis-equilibria, which cannot be explained by other physical non-equilibrium processes like photodissociation ("biosignatures"). The aim of this letter is to propose a robust criterion for step one. We define a non-equilibrium marker as a combination of (i) a given molecule with (ii) one of H_2O, CH_4 or CO_2, which both can react exothermally. Such pairs of molecules populate the opposite corners in Fig. 1 and have practically zero overlap in equilibrium. Examples of such pairs of reactants in exothermal reactions are listed in Sect. 2.

Krissansen-Totton et al. (2019) proposed the simultaneous detection of CH_4 and CO_2 (without CO) as a biosignature, arguing that only biological fluxes are high enough to replenish CH_4 in the upper atmospheres where it is rapidly destroyed by photochemical processes. However, this study has shown that CH_4 and CO_2 can coexist in chemical equilibrium in type C atmosphere, which could lead to many false positive detections. The outgassing from warm common rocks provides a natural mechanism to generate equilibrated mixtures of CH_4 and CO_2 with only trace amounts of CO, and at $T \gtrsim 400$ K, type C atmospheres may contain equally large concentrations of H_2O, CH_4 and CO_2 in chemical equilibrium. At $T \approx 350$ K, liquid water can coexist beside arbitrary concentrations of CH_4 and a concentration of CO_2 of the order of a few percent. It would be important to re-evaluate photochemical effects in type C atmospheres, where there is no free oxygen available and, therefore, the reaction products of CH_4 are more likely to just reform CH_4.

Acknowledgements. P. W. and Ch. H. acknowledge funding from the European Union H2020-MSCA-ITN-2019 under Grant Agreement no. 860470 (CHAMELEON). O. H. acknowledges the PhD stipend form the University of St Andrews' Centre for Exoplanet Science. P. B. acknowledges support from the St Leonards interdisciplinary scholarship.

References

Arney, G., Domagal-Goldman, S. D., Meadows, V. S., et al. 2016, Astrobiology, 16, 873, pMID: 27792417
Chase, M. W. 1986, JANAF thermochemical tables (American Chemical Society; New York)
Chase, M. W., Curnutt, J. L., Downey, J. R., et al. 1982, in Journal of Physics Conference Series, Vol. 11, Journal of Physics Conference Series, 695–940
Gaudi, B. S., Seager, S., Mennesson, B., et al. 2018, arXiv e-prints, arXiv:1809.09674
Heng, K. & Tsai, S.-M. 2016, ApJ, 829, 104
Herbort, O., Woitke, P., Helling, C., & Zerkle, A. 2020, A&A, 636, A71
Hu, R. & Seager, S. 2014, ApJ, 784, 63
Krissansen-Totton, J., Arney, G. N., Catling, D. C., et al. 2019, BAAS, 51, 158
Krissansen-Totton, J., Olson, S., & Catling, D. C. 2018, Science Advances, 4, eaao5747
Meadows, V. S., Reinhard, C. T., Arney, G. N., et al. 2018, Astrobiology, 18, 630
Miller, S. L. 1953, Science, 117, 528
Misra, A., Krissansen-Totton, J., Koehler, M. C., & Sholes, S. 2015, Astrobiology, 15, 462, pMID: 26053611
Morley, C. V., Kreidberg, L., Rustamkulov, Z., Robinson, T., & Fortney, J. J. 2017, ApJ, 850, 121
Moses, J. I., Line, M. R., Visscher, C., et al. 2013, ApJ, 777, 34
Niemann, H. B., Atreya, S. K., Bauer, S. J., et al. 2005, Nature, 438, 779
Sandora, M. & Silk, J. 2020, MNRAS, 495, 1000
Seager, S., Bains, W., & Hu, R. 2013, ApJ, 777, 95
Sousa-Silva, C., Seager, S., Ranjan, S., et al. 2020, Astrobiology, 20, 235, pMID: 31755740
Stüeken, E., Kipp, M., Koehler, M., et al. 2016, Astrobiology, 16, 949, pMID: 27905827
Turbet, M., Bolmont, E., Bourrier, V., et al. 2020, arXiv e-prints, arXiv:2007.03334
Waite, J. H., Glein, C. R., Perryman, R. S., et al. 2017, Science, 356, 155
Woese, C. R. & Fox, G. E. 1977, Proceedings of the National Academy of Science, 74, 5088
Woitke, P., Helling, C., Hunter, G. H., et al. 2018, A&A, 614, A1
Zerkle, A. L., Claire, M. W., Domagal-Goldman, S. D., Farquhar, J., & Poulton, S. W. 2012, Nature Geoscience, 5, 359

Appendix A: Type A, B and C atmospheres

In the following, we systematically list the principle molecular composition and approximate abundances expected for low-temperature gases in chemical equilibrium. These results are entirely given by the element abundances and the stoichiometric factors of the thermodynamically most favourable molecules, and are hence independent of pressure and temperature.

Appendix A.1: Type A atmospheres

Type A atmospheres are H-rich and occur for $H > 2\,O + 4\,C$ (Eq. 6). They are featured by the stability of NH_3. Since N_2 can react exothermally with H_2

$$N_2 + 3\,H_2 \quad \longrightarrow \quad 2\,NH_3 \qquad : -0.81\,\mathrm{eV}\,, \qquad \text{(A.1)}$$

we have either a combination of NH_3 and H_2 (type A1) or a combination of NH_3 and N_2 (type A2), depending on nitrogen abundance.

Type A1 atmospheres mainly contain H_2O, CH_4, NH_3 and H_2, and occur for $H > 2\,O + 4\,C$ and low nitrogen abundance $3N < H - 2\,O - 4\,C$. Based on these molecules' stoichiometry, following the same procedure as outlined in Sect. 2, the expected low-temperature abundances in chemical equilibrium are

$$\begin{aligned} \frac{p_{\mathrm{H2O}}}{p_{\mathrm{gas}}} &= \frac{2\,O}{H - N - 2\,C}\,, & \frac{p_{\mathrm{CH4}}}{p_{\mathrm{gas}}} &= \frac{2\,C}{H - N - 2\,C}\,, \\ \frac{p_{\mathrm{NH3}}}{p_{\mathrm{gas}}} &= \frac{2\,N}{H - N - 2\,C}\,, & \frac{p_{\mathrm{H2}}}{p_{\mathrm{gas}}} &= \frac{H - 2\,O - 4\,C - 3\,N}{H - N - 2\,C}\,. \end{aligned} \qquad \text{(A.2)}$$

Type A2 atmospheres mainly contain H_2O, CH_4, NH_3 and N_2, and occur for $H > 2\,O + 4\,C$ and high nitrogen abundance $3N > H - 2\,O - 4\,C$. The expected low-temperature abundances in chemical equilibrium are

$$\begin{aligned} \frac{p_{\mathrm{H2O}}}{p_{\mathrm{gas}}} &= \frac{6\,O}{H + 2\,C + 3\,N + 4\,O}\,, & \frac{p_{\mathrm{CH4}}}{p_{\mathrm{gas}}} &= \frac{6\,C}{H + 2\,C + 3\,N + 4\,O}\,, \\ \frac{p_{\mathrm{NH3}}}{p_{\mathrm{gas}}} &= \frac{2\,H - 8\,C - 4\,O}{H + 2\,C + 3\,N + 4\,O}\,, & \frac{p_{\mathrm{N2}}}{p_{\mathrm{gas}}} &= \frac{3\,N + 4\,C + 2\,O - H}{H + 2\,C + 3\,N + 4\,O}\,. \end{aligned} \qquad \text{(A.3)}$$

Figure A.1 shows the concentrations of NH_3, H_2 and N_2 in chemical equilibrium in type A atmospheres. The left parts of these plots, where $(N - H_{\mathrm{eff}})/(N + H_{\mathrm{eff}}) < -0.5$, correspond to type A1, and the right parts $(N - H_{\mathrm{eff}})/(N + H_{\mathrm{eff}}) > -0.5$ correspond to type A2. We have used an effective H abundance here, $H_{\mathrm{eff}} = H - 2\,O - 4\,C$ in order to plot the results with regard to the hydrogen abundance still available after H_2O and CH_4 formation. Comparison with a large sample of models, systematically varying all H, C, N, O abundances (see dots in Fig. A.1), shows that the low-temperature expectations according to Eqs. (A.2) and (A.3) require temperatures $T \lesssim 300$ K to be accurate, which differs from type B and type C atmospheres, where the low-temperature expectations are accurate up to $T \lesssim 600$ K. The reason for the earlier occurrence of deviations of the model results from their low-temperature expectations is that reaction (A.1) is only mildly exothermic, so the entropy terms kick in sooner when increasing the temperature. Thus, the low-temperature expectations in type A atmospheres are far less useful as compared to type B and type C atmospheres, where they are more robust and hence more suitable for classification. However, the borderline between type C and type A atmospheres, and the prediction of H_2O and CH_4 concentrations remains robust even in type A atmospheres.

Both type A1 and type A2 atmospheres can contain water clouds if temperatures are sufficiently low, but no graphite (soot) clouds, and only traces of CO_2, O_2 and CO molecules in chemical equilibrium.

Appendix A.2: Type B atmospheres

Type B atmospheres are oxygen-rich and occur for $2\,O > H + 4\,C$ (Eq. 5). They mainly contain H_2O, CO_2, N_2 and O_2. With similar stoichiometric arguments as presented in Sect. 2, the expected low-temperature abundances in chemical equilibrium are

$$\begin{aligned} \frac{p_{\mathrm{H2O}}}{p_{\mathrm{gas}}} &= \frac{2\,H}{H + 2\,O + 2\,N}\,, & \frac{p_{\mathrm{CO2}}}{p_{\mathrm{gas}}} &= \frac{4\,C}{H + 2\,O + 2\,N}\,, \\ \frac{p_{\mathrm{N2}}}{p_{\mathrm{gas}}} &= \frac{2\,N}{H + 2\,O + 2\,N}\,, & \frac{p_{\mathrm{O2}}}{p_{\mathrm{gas}}} &= \frac{2\,O - H - 4\,C}{H + 2\,O + 2\,N}\,. \end{aligned} \qquad \text{(A.4)}$$

Type B atmospheres can contain water clouds if temperatures are sufficiently low, but no graphite (soot) clouds, and only traces of CH_4, H_2, NH_3 and CO molecules in chemical equilibrium.

Appendix A.3: Type C atmospheres

Type C atmospheres have been discussed in Sect. 2. They occur in the triangle between the conditions listed by Eqs. (5) to (7). The main molecules are H_2O, CO_2, CH_4 and N_2 with low-temperature concentrations approximately given by Eq. (4). Type C atmospheres can contain water and graphite (soot) clouds if temperatures are sufficiently low, but only traces of O_2, H_2, NH_3 and CO molecules in chemical equilibrium.

Appendix B: Variation of temperature, pressure, and nitrogen abundance

Figures B.1 ($T = 300$ K) and B.2 ($T = 600$ K) show the effects of temperature. The cold case is very pure and the molecular concentrations are very close to Eq. (4), with negligible concentrations of all trace molecules in all type A, B and C atmospheres. The warmer model shows notable concentrations of H_2 and CO in type C atmospheres, but without much feedback on the main molecules, as already discussed in Table 2.

Figures B.3 ($p = 0.01$ bar) and B.4 ($p = 100$ bar) show that the pressure has practically no influence on the results, except for the trace concentrations of H_2 and CO in type C atmospheres.

Figures B.5 ($N = 0.001$) and B.6 ($N = 0.5$) show the small influence of the nitrogen abundance on the results, when we plot the concentrations after subtraction of N_2 from the total particle density. For type B and C atmospheres, this works perfectly well, because most nitrogen forms N_2 in equilibrium, and the results for varying N-abundance in type B and C atmospheres are virtually indistinguishable. However, for type A atmospheres, the results actually depend on N, with sub-types A1 and A2 as explained in Appendix A, and the results would better be plotted in a three dimensional way. Hence, Figs. B.5 and B.6 only provide cuts through this 3D space, at selected N-abundances, for type A atmospheres in the lower left corner.

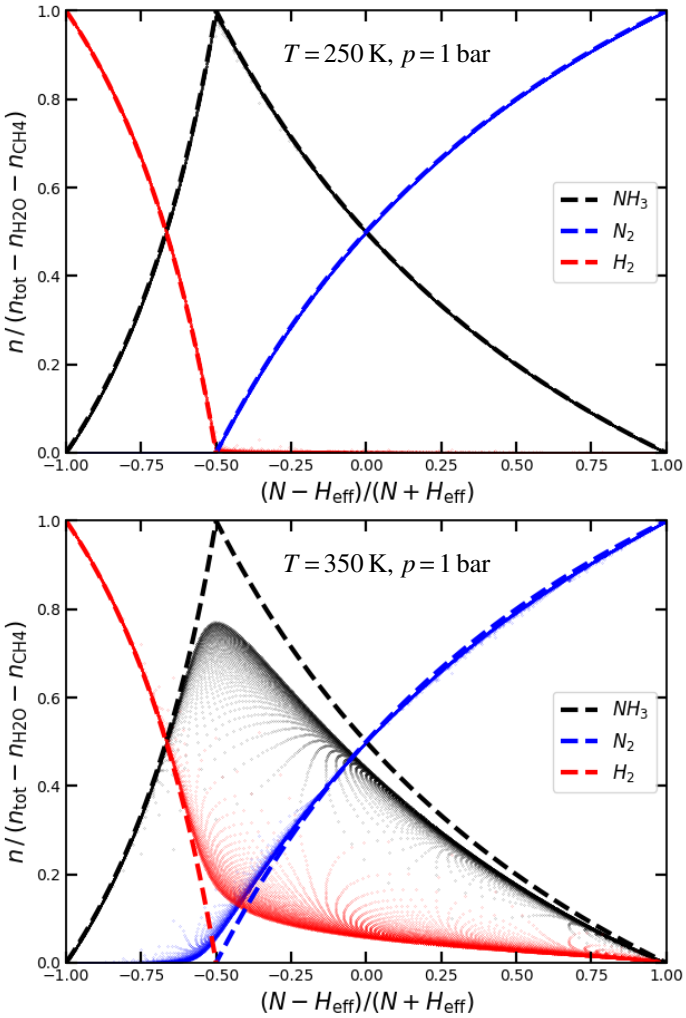

Fig. A.1. Concentrations of NH_3, N_2 and H_2 in chemical equilibrium in type A atmospheres. $H_{\rm eff} = H - 2\,O - 4\,C$ is the H element abundance remaining after subtraction of H_2O and CH_4. The dashed lines are the low-temperature expectations according to Eqs. (A.2) and (A.3). The dots are taken from a wide range of models, systematically varying all H, C, N, O element abundances at $p = 1$ bar, for $T = 250$ K (top plot) and for $T = 350$ K (bottom plot).

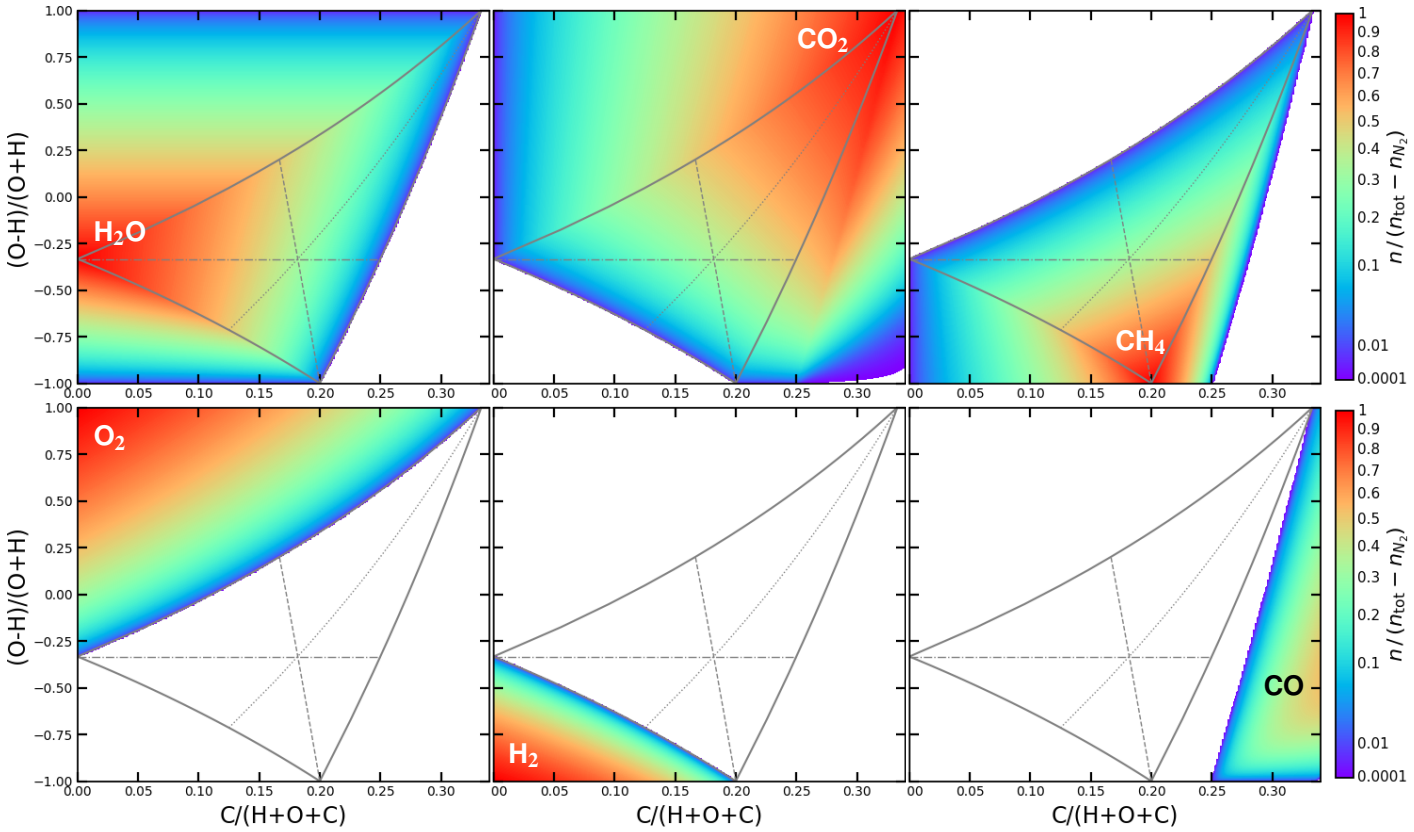

Fig. B.1. Same as Fig. 1, but for $T = 200\ K$, $p = 1$ bar, and $N = 0.001$.

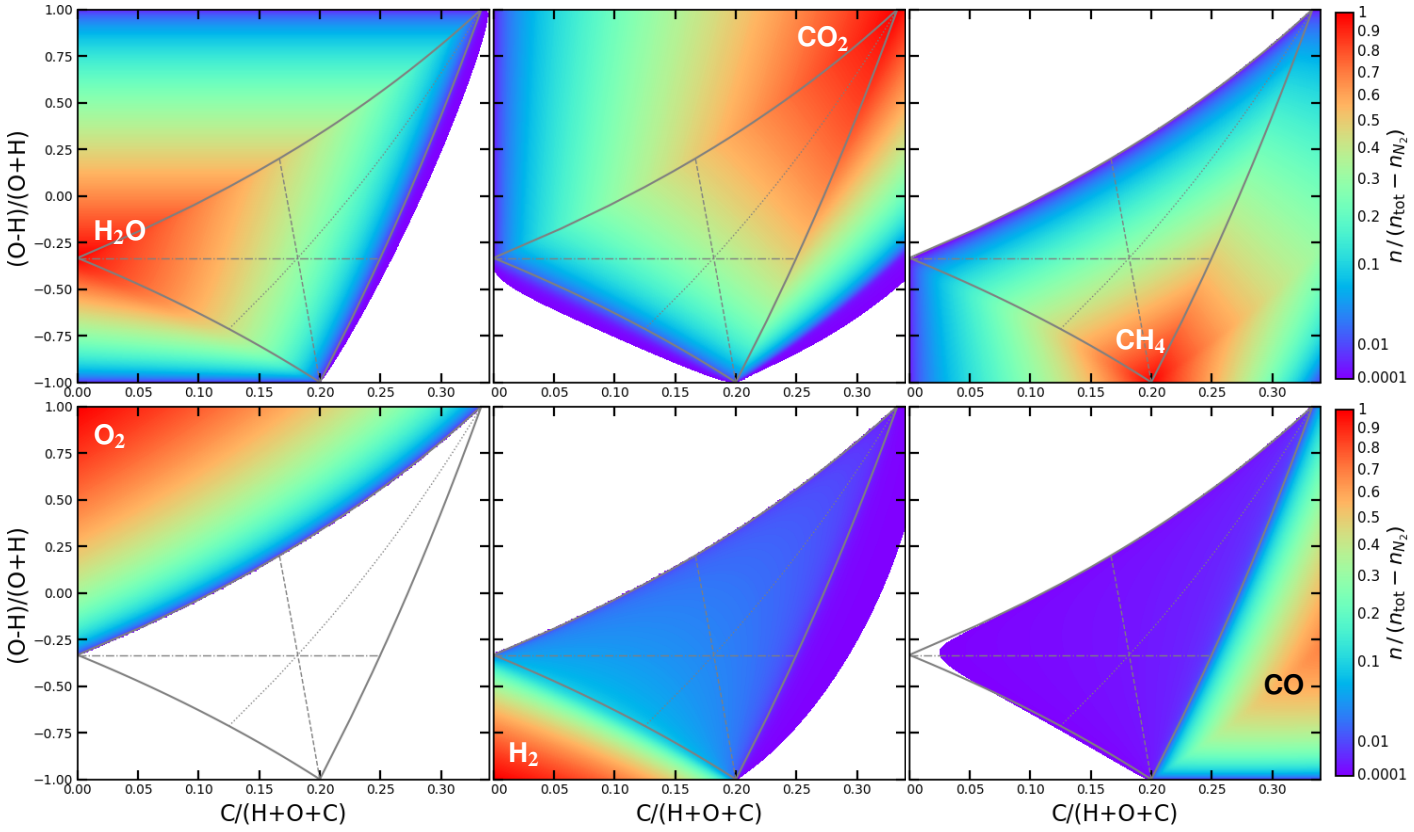

Fig. B.2. Same as Fig. 1, but for $T = 600\ K$, $p = 1$ bar, and $N = 0.001$.

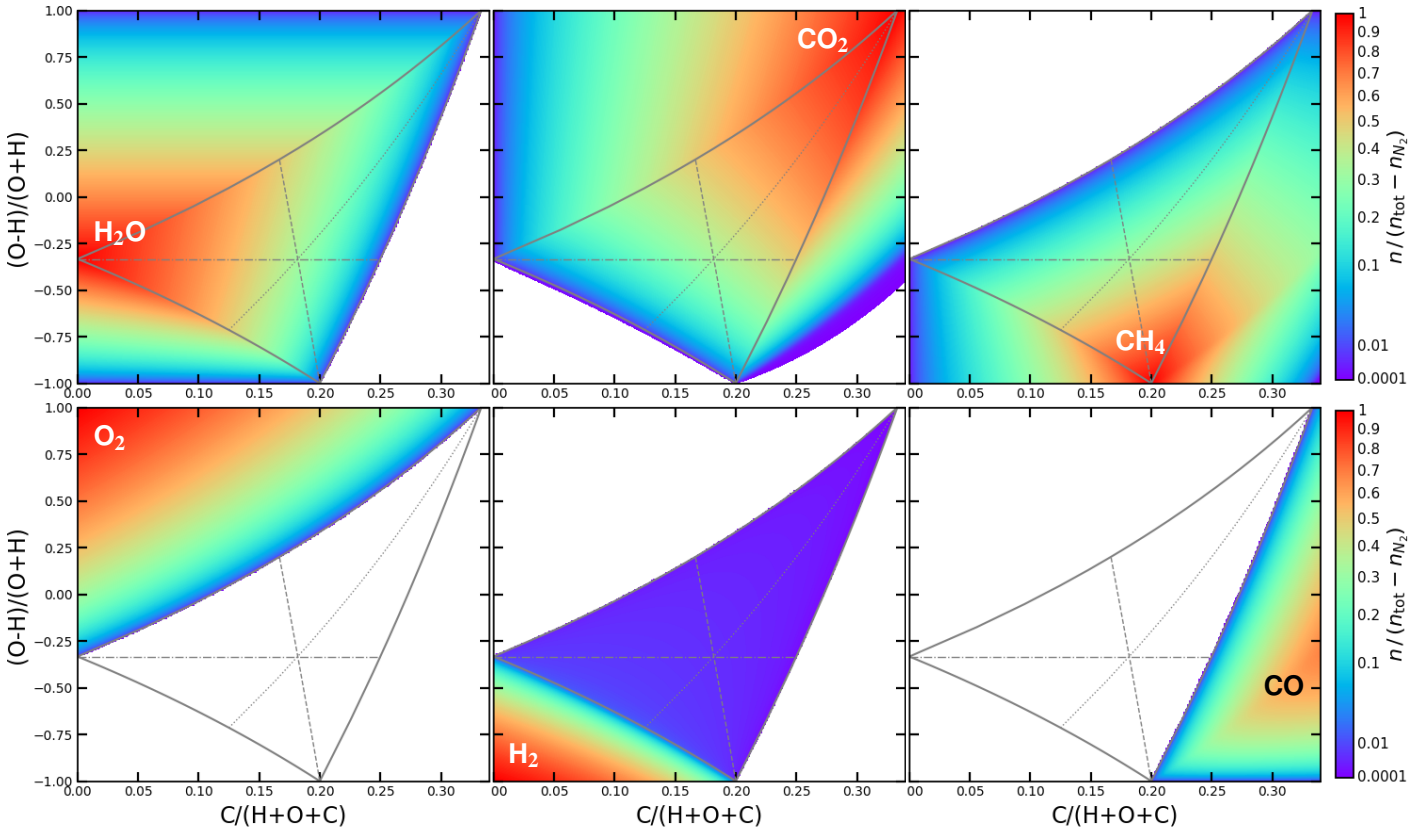

Fig. B.3. Same as Fig. 1, but for $T = 400\,K$, $p = 0.01$ bar, and $N = 0.001$.

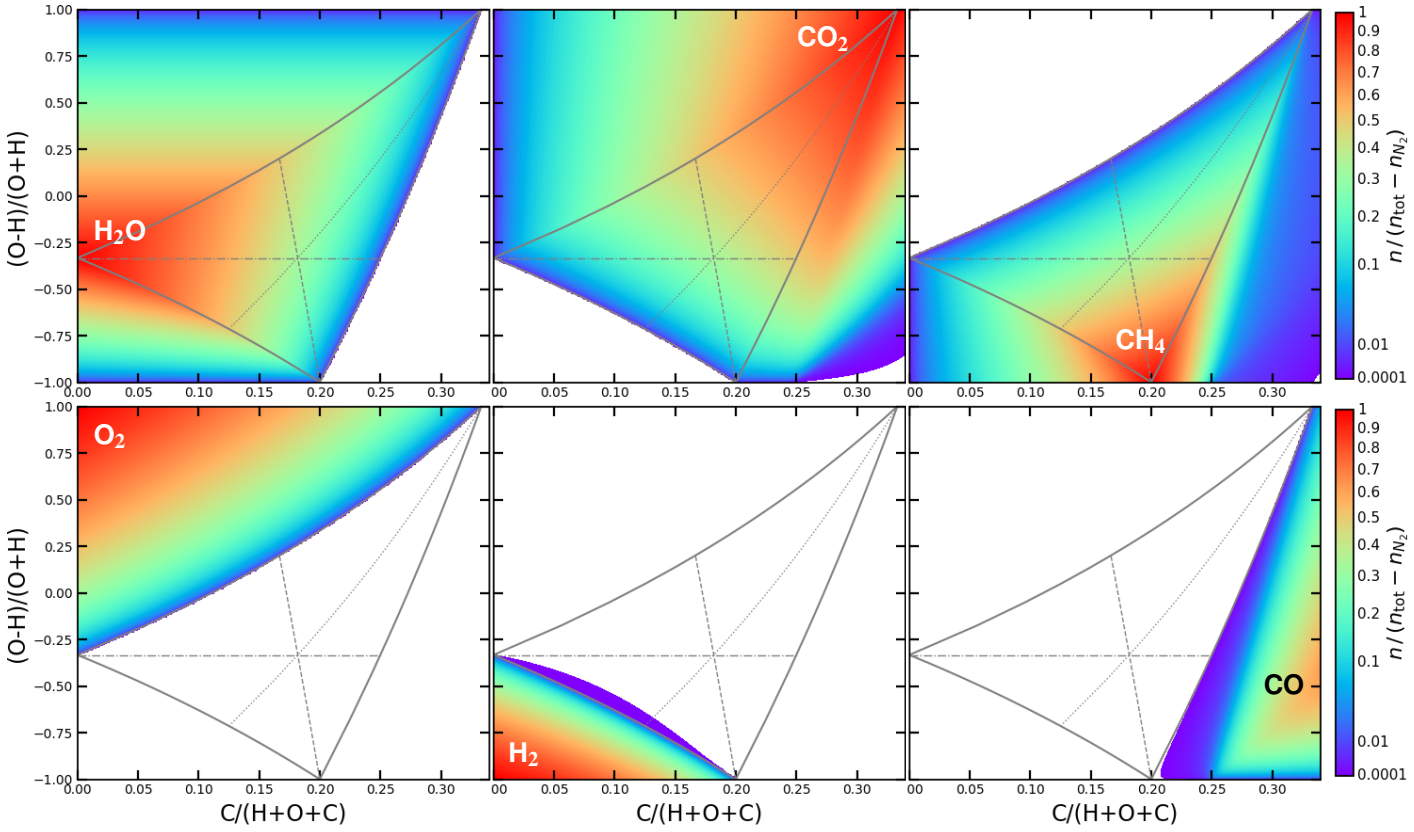

Fig. B.4. Same as Fig. 1, but for $T = 400\,K$, $p = 100$ bar, and $N = 0.001$.

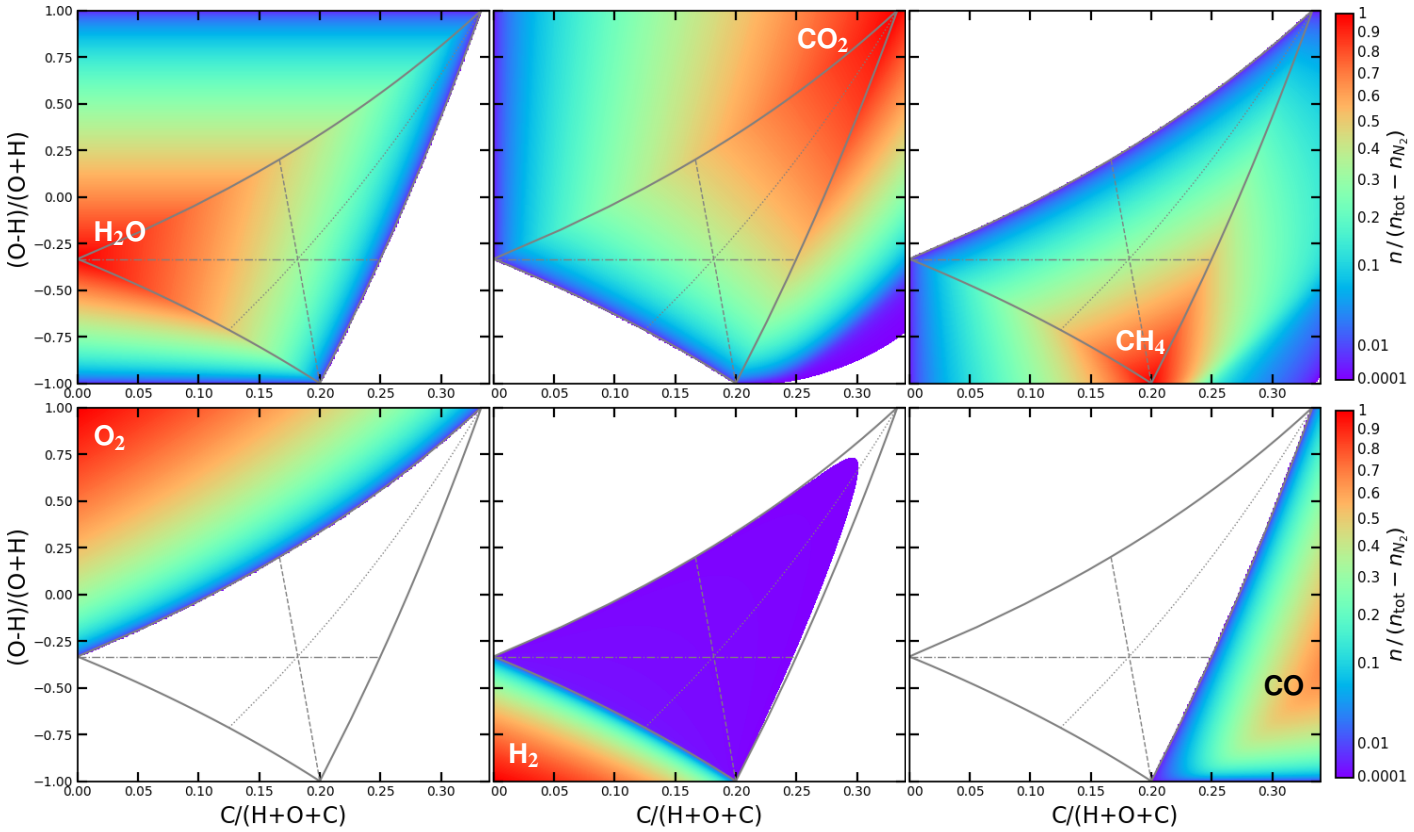

Fig. B.5. Same as Fig. 1, $T = 400\ K$, $p = 1$ bar, and $N = 0.001$.

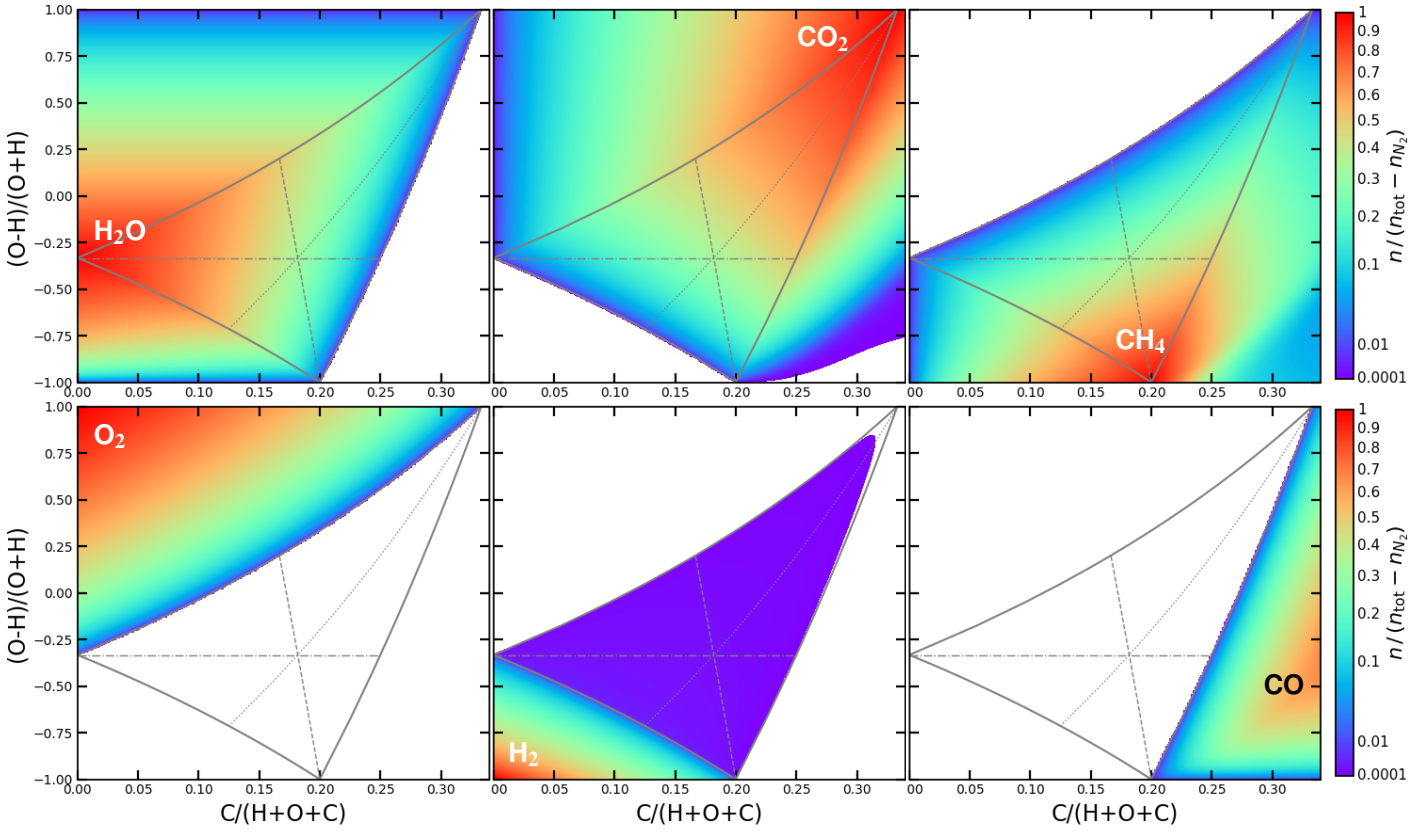

Fig. B.6. Same as Fig. 1, but for $T = 400\ K$, $p = 1$ bar, and $N = 0.5$.